Monolayers

Deutsche Ausgabe: DOI: 10.1002/ange.201509285
Internationale Ausgabe: DOI: 10.1002/anie.201509285

Synthesis of Atomically Thin Boron Films on Copper Foils

Guoan Tai, Tingsong Hu, Yungang Zhou, Xufeng Wang, Jizhou Kong, Tian Zeng, Yuncheng You, and Qin Wang*

Abstract: *Two-dimensional boron materials have recently attracted extensive theoretical interest because of their exceptional structural complexity and remarkable physical and chemical properties. However, such 2D boron monolayers have still not been synthesized. In this report, the synthesis of atomically thin 2D γ-boron films on copper foils is achieved by chemical vapor deposition using a mixture of pure boron and boron oxide powders as the boron source and hydrogen gas as the carrier gas. Strikingly, the optical band gap of the boron film was measured to be around 2.25 eV, which is close to the value (2.07 eV) determined by first-principles calculations, suggesting that the γ-B_{28} monolayer is a fascinating direct band gap semiconductor. Furthermore, a strong photoluminescence emission band was observed at approximately 626 nm, which is again due to the direct band gap. This study could pave the way for applications of two-dimensional boron materials in electronic and photonic devices.*

Two-dimensional (2D) materials are attractive components of atomic-layer field-effect transistors (FETs), sensors, and photovoltaic and photoelectric devices.[1–5] Although graphene has been shown to be a useful material for high-performance electronics owing to its very high carrier mobility, it suffers from the lack of a significant band gap, which limits its application in digital electronics.[3–5] Hence, three-atom-thick 2D semiconducting transition-metal dichalcogenides (TMDs; e.g., MoS_2, WS_2, $MoSe_2$, WSe_2) and one-atom-thick non-metal/metal layers with a honeycomb structure (e.g., silicene, germanene, phosphorene, arsenene, antimonene, and stannene) have attracted wide interest.[3–7] Nevertheless, the stoichiometry of 2D TMD materials is particularly challenging to control during growth by chemical vapor deposition (CVD).[8,9] 2D elemental semiconductor materials, such as phosphorene and silicene, are unstable in air, which restricts their applications in photoelectric and photovoltaic devices.[9,10] Therefore, it is extremely interesting to develop a novel elemental semiconductor with high stability in air.

Recently, elemental boron has received significant attention owing to its fascinating physical and chemical properties, such as exceptional structural complexity, superhardness, partial ionic bonding, superconductivity, thermoelectricity, and high chemical stability.[11,12] It has at least 16 polymorphs, such as α-B_{12}, β-B_{106}, T-B_{192}, and γ-B_{28}, which are often prepared at high temperature and pressure.[12,13] Atomically thin 2D boron films have received extensive theoretical interest in recent years. Early theoretical predictions suggested that small boron clusters exhibit quasi-planar structures called "borophene", but that unstable boron sheets tend to form buckled all-triangular lattices.[13] Very recently, various forms of monolayered boron structures, consisting of triangular lattices with hexagonal vacancies, have been proposed with different vacancy densities and arrangements.[14–16] To date, however, such extended 2D boron monolayers have not been realized experimentally.

Herein, we grew large, atomically thin 2D γ-boron films on copper (Cu) foils by CVD using a mixture of boron and boron oxide powders as the boron source and hydrogen gas as the carrier gas. The structure of the obtained thin film was characterized by high-resolution transmission electron microscopy (HRTEM), and its optical properties were analyzed by UV/Vis absorption and photoluminescence spectroscopy. We also performed first-principles calculations of the electronic band structure, which showed that the γ-B_{28} monolayer is a fascinating direct band gap semiconductor. Unlike for graphene or other 2D atomic layers that can be exfoliated from their bulk samples and show weak interlayer binding, such bulk boron materials do not exist in nature. Therefore, this study could open the door to further investigations of its exciting properties and applications in electronic and photonic devices.

The growth procedure adopted for the boron thin films is shown in Figure 1a. We prepared the thin films by using a home-made two-zone CVD furnace. To control the growth rate, the temperatures of the source zone (T_1) and the substrate zone (T_2) were separately controlled (Supporting Information, Figure S1). Prior to the growth, a 25 μm thick piece of Cu foil was annealed at 1000 °C for one hour to smoothen the surface of the foil and enlarge the grain boundaries. To obtain the diboron dioxide (B_2O_2) vapor by annealing a mixture of B and B_2O_3 powders, T_1 was set to

[*] Prof. G. Tai, T. S. Hu, X. F. Wang, Dr. J. Z. Kong, T. Zeng
The State Key Laboratory of Mechanics and Control of Mechanical Structures, Laboratory of Intelligent Nano Materials and Devices of Ministry of Education, College of Aerospace Engineering
Nanjing University of Aeronautics and Astronautics
Nanjing 210016 (China)
E-mail: taiguoan@nuaa.edu.cn

T. S. Hu, X. F. Wang, T. Zeng, Y. C. You, Q. Wang
School of Material Science and Technology
Nanjing University of Aeronautics and Astronautics
Nanjing 210016 (China)

Dr. Y. G. Zhou
School of Physical Electronics
University of Electronic Science and Technology of China
Chengdu, 610054 (China)

Dr. J. Z. Kong
College of Mechanical and Electrical Engineering
Nanjing University of Aeronautics and Astronautics
Nanjing 210016 (China)

Supporting information and ORCID(s) from the author(s) for this article are available on the WWW under http://dx.doi.org/10.1002/anie.201509285.

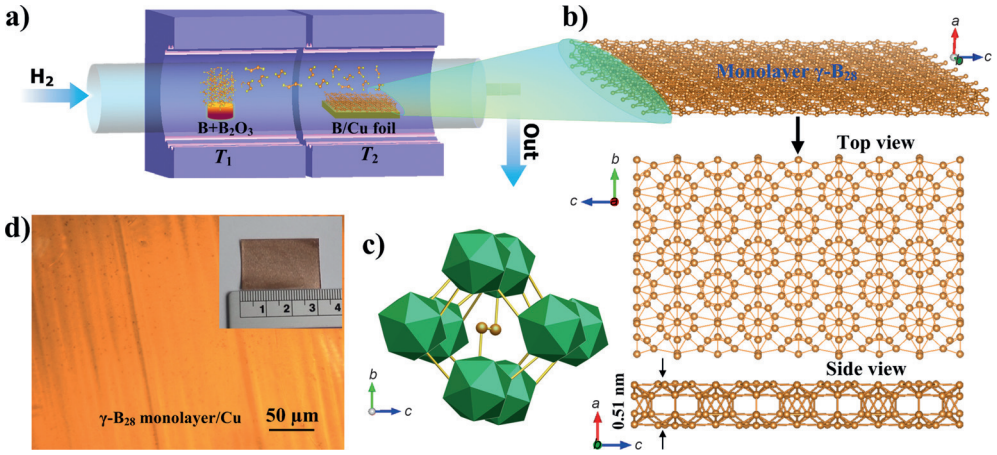

Figure 1. a) Schematic representation of the home-made two-zone furnace used to obtain atomically thin 2D γ-B_{28} films by CVD. b) Top and side views of the monolayer. Unit cell vectors are shown. c) Polyhedral structure of the basic unit cell of the monolayer shown in *bc* projection. Boron atoms forming dumbbells are shown as orange spheres. d) Optical image of a monolayer on Cu foil. Inset: photograph of the monolayer on Cu foil.

1100 °C. After the thin films had been prepared by heating to 1000 °C (T_2) for one hour, they were transferred onto different substrates for further characterization and application (see the Methods Section in the Supporting Information).

The structure of the thin film is composed of icosahedral B_{12} units and B_2 dumbbells (Figure 1 b).[12,17,18] It features orthorhombic γ-B_{28} cells with a unit cell of 28 atoms (a = 5.054, b = 5.620, c = 6.987 Å) and the space group *Pnnm*, and it can be regarded as a boron boride $(B_2)^{\sigma+}(B_{12})^{\sigma-}$ because of the charge transfer between these two components.[12] The polyhedral structure of the basic unit cell of the monolayer is shown in *bc* projection in Figure 1 c.[17] The structure is built of B_{12} icosahedra linked into a 3D network by B_2 dumbbells: The dumbbells are aligned almost parallel to the *a* axis, and nearly rectangular channels along the axis are filled with boron chains.

A boron thin film was controllably prepared over the entire surface of a Cu foil with a size of 2 × 3 cm^2 (Figure 1 d); it could then be easily transferred onto a 285 nm thick SiO_2/Si substrate by removing the Cu foil using dilute ferric chloride ($FeCl_3$) solution. An optical image of the film on the 285 nm thick SiO_2/Si substrate indicates that it has a large area and is continuous (Figure 2 a; for the corresponding photograph of the film on the 1 × 1 cm^2 substrate, see Figure 2 a).

To estimate the thickness and determine the atomic structure of the thin film, atomic force microscopy (AFM) and transmission electron microscopy (TEM) were employed. A typical AFM image shows that the thickness of the boron film is around 0.80 nm (Figure 2 b); this value is close to the *a* axis height of the monolayer γ-B_{28} model (a = 0.5054 nm; side view in Figure 1 b), which indicates that the obtained boron film was a monolayer. A TEM image shows the morphology of a boron film covering the whole surface of the TEM grid (Figure 2 c), and a TEM image of a thin film with a folded edge is shown in Figure 2 c, inset, further confirming that the film was monolayer. We observed that the boron film grown on a Cu foil was of polycrystalline nature with small grains and highly concentrated grain boundaries and defects, similar to *h*-BN films.[19] In sharp contrast to the graphene layers obtained by copper-catalyzed CVD growth, the nucleation density of boron on Cu foils was much higher, which might be due to the high chemical affinity of boron-containing intermediate species to the Cu surface.[16] The atomic arrangement of the B atoms could not be clearly observed owing to the damage caused by electrons subjected to an acceleration

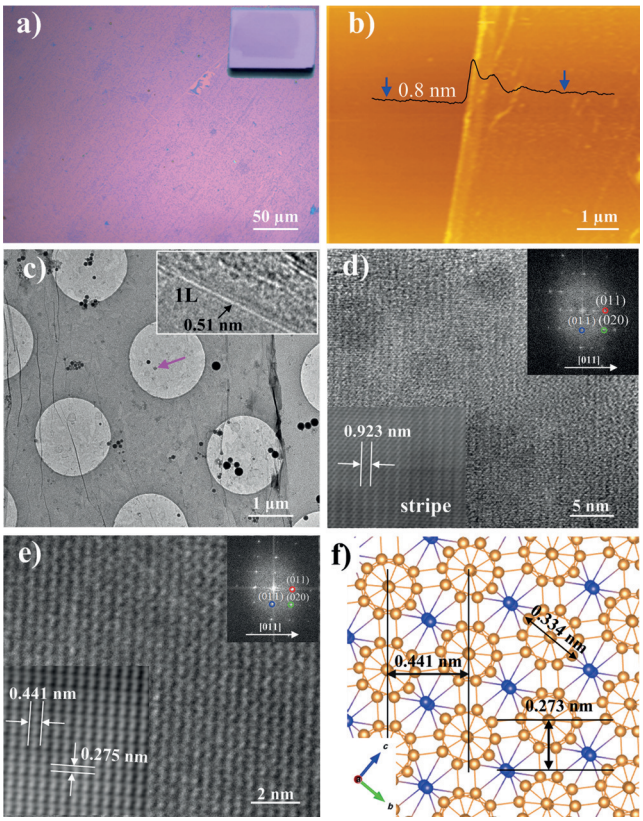

Figure 2. a) Optical image of monolayer γ-B_{28} on a 285 nm thick SiO_2/Si substrate. Inset: corresponding photograph. b) AFM topographical image of a monolayer on the 285 nm SiO_2/Si substrate. Height analysis along the black line in the inset indicates a thickness of 0.80 nm, suggesting that the film is monolayer. c) Low-resolution TEM image of the film transferred onto the holes of a Cu net. Inset: typical TEM image of the film with a folded edge. 1L indicates one layer. d) HRTEM image. The insets in the top right and bottom left corners are FFT and reconstructed FFT images, respectively. e) HRTEM image of the thick region indicated by the pink arrow shown in (c). Insets are similar to those in (d). f) Structure of γ-B_{28}; the two oppositely charged sublattices are shown in different colors (anionic orange; cationic blue).

voltage of 200 kV, as required for HRTEM analysis,[20] but a fast Fourier transform (FFT) image shows the high crystallinity of the layer and features characteristic of an orthorhombic structure; the three FFT spots can be indexed to the (011), (01$\bar{1}$), and (020) crystal faces of orthorhombic γ-B_{28} (Figure 2 d, inset in the top right corner).[12] The HRTEM image was reconstructed by masking the FFT pattern. Longitudinal 1D stripes were clearly observed in the HRTEM image, and each stripe with a width of 0.923 nm was composed of two alternating (011) lattice planes, indicating that the structure of the thin film has *Pnnm* characteristics (Figure 2 d, inset in the bottom left corner). To more clearly analyze the structure, we performed HRTEM analysis on the thick region marked by a pink arrow in Figure 2 c, as shown in Figure 2 e. The HRTEM images can be interpreted in terms of a combination of boron spheres because the measured diameter of the spheres (ca. 3.05–3.82 Å) in the HRTEM image is comparable to that of the circumscribed circle around the B_{12} icosahedron (3.34 Å; see Figure 2 f).[17] The FFT and HRTEM images clearly reveal the lattice structure of the monolayer with two lattice *d* spacings of approximately 0.441 and 0.275 nm, which correspond to the (011) and (01$\bar{1}$) crystal faces of orthorhombic γ-B_{28}.[12,17] The results are in good agreement with the structural parameters obtained by single-crystal/powder X-ray diffraction and those from first-principles calculations (Figure 2 f).[12,17,18]

Raman spectra were obtained for the boron monolayer on copper foil in the spectral range of 200–1200 cm^{-1} (Figure 3 a). Compared with blank Cu foil, the monolayer γ-B_{28} film on Cu foil gave rise to one characteristic band centered at approximately 618 cm^{-1}. The band corresponds to the A_g breathing mode of the B_{12} icosahedra.[21,22] We did not observe the band corresponding to pure B_2O_3 at about 806 cm^{-1}, which would arise from the symmetric breathing vibration of the boroxole rings.[23] Likewise, no bands characteristic of B_2O_2 were detected (Figure S2). For comparison, a Raman spectrum of bulk β-rhombohedral boron was recorded (Figure 3 b). Evidently, the Raman spectrum of bulk β-B is completely different from that of the monolayer obtained in our experiments.

X-ray photoelectron spectroscopy (XPS) was used to investigate the chemical state of boron in the film (Figure 3 c, d). The XPS survey-scan spectrum of the film on a Cu foil for binding energies from 0 to 1200 eV is shown in Figure 3 c. Aside from the B peak, peaks corresponding to Cu, C, and O were also detected. The Cu peak is due to the Cu substrate. The C and O species may arise from impurities in the vacuum vessels, which unavoidably leak into the chamber from the external environments. The binding energy of the B 1s core-level electrons gives rise to a single peak centered at 187.6 eV, which corresponds to the B–B bond (Figure 3 d).[24,25]

The monolayer γ-B_{28} thin films on Cu foil were synthesized as follows: A mixture of B and B_2O_3 powders was heated at 1100 °C to form vaporized B_2O_2 dimers, which had been analyzed by earlier mass-spectroscopic measurements;[26] then, the vapor was reduced to boron by high-purity H_2 gas and deposited on the Cu foil at a lower temperature of about 1000 °C. The formation of the nearly uniform monolayer over the whole Cu surface, which is attributed to the poor solubility of boron in copper, can be interpreted in terms of a surface-catalyzed process.[27] According to solid-state crystal theory, the B_2O_2 vapor should come into contact with the nearly melted Cu and be reduced to elemental boron on the Cu surface by the reductant, H_2 gas. The deposited boron would begin to dissolve and diffuse into the catalytic Cu surface. Once the system reaches supersaturation, the boron would nucleate as the thin film to counteract the continuous feeding of B onto the surface.

To fully understand the growth mechanism of the atomic layers, a systematic analysis of the growth kinetics is needed. We analyzed the growth of the films on Cu foil as a function of reaction time under isothermal and isobaric conditions. At a given temperature, the films gradually became thin with time, which was easily observed by analyzing the optical contrast between the films and the 285 nm thick SiO_2/Si substrates (Figure S3 a–d). Furthermore, they were also transformed from amorphous into crystalline species, as determined by HRTEM and FFT analysis (Figure S3 e–h). For durations of less than 15 min, the thin films were relatively thick and amorphous. After more than 30 min, polycrystalline thin films were observed, as confirmed by the lattice textures observed by HRTEM and the corresponding FFT image. The FFT image was taken from a region with lots of small crystal grains in

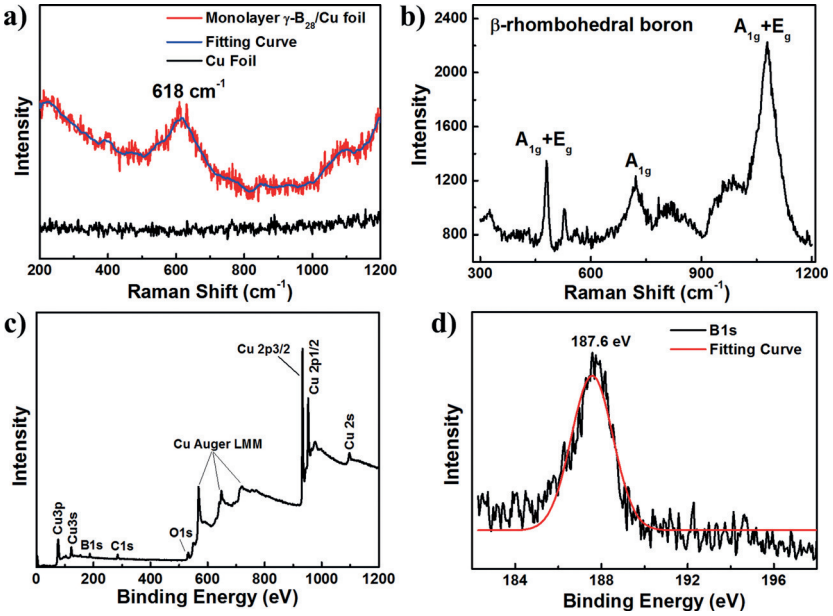

Figure 3. a) Raman spectra of a monolayer γ-B_{28} film on Cu foil (red) and a blank Cu foil (black). b) Raman spectrum of bulk β-rhombohedral boron. c) XPS survey-scan spectrum of a boron film on Cu foil, showing the B 1s, C 1s, O 1s, and Cu peaks. b) XPS analysis of the B 1s peak.

the HRTEM image, and the primary ring diffraction pattern induced by the polycrystalline species can be indexed to orthorhombic γ-B_{28} (Figure S3 f, inset). However, the diffraction intensity is not uniform over several rings, indicating preferential orientation or texture structure in the film. The stepwise development of the film according to HRTEM and FFT analysis suggests that large quantities of amorphous boron may be microcrystalline deposits of this particular polymorph of the element.[28] When the reaction was allowed to proceed for 60 min, a uniform monolayer was obtained (Figure 2 a).

The growth of continuous monolayers was inhibited by a reduced pressure down to 18 Pa or an increased pressure up to 100 Pa (Figure S4 a, b). Moreover, the surface temperature of the Cu foils was decreased just enough to reduce the mobility of the surface atoms so that much thicker boron films were formed (Figure S4 c, d). We thus conclude that amorphous boron is converted into a readily identifiable crystalline form by a surface diffusion mechanism.

The optical properties of the γ-B_{28} monolayer on a quartz substrate were analyzed by UV/Vis absorption spectroscopy (Figure 4 a). A characteristic absorption peak, λ_{onset}, was observed at 614 nm (phonon energy 2.05 eV), which could be attributed to a direct excitonic transition. The corresponding optical band gap ($E_{g,op}$) was estimated to be 2.25 eV according to $(\alpha h\nu)^2 = h\nu - E_g$, where $h\nu$ is the corresponding phonon energy, and α is the absorbance. This value is much higher than that of the corresponding bulk phase measured either by near-infrared optical absorption spectroscopy or calculated by first-principles calculations (1.7 eV), which is due to the presence of strong quantum-confinement effects in the monolayer.[18] In agreement with the UV/Vis spectrum, the room-temperature photoluminescence (PL) spectrum shows a large, sharp emission band centered at 626 nm with a very narrow full width at half maximum of about 22 nm (Figure 4 b). The PL peak can be attributed to the recombination of free excitons, which represents lower boundaries on the fundamental band gap value. For comparison, the PL spectrum of a bulk β-B sample was measured because the band gap of bulk β-B is close to that of bulk γ-B_{28}, and both of their band gaps are indirect.[12,18] A weak emission band centered at 684 nm was observed, and the remarkable blue shift of about 58 nm in the PL spectra could be ascribed to strong quantum-confinement effects in the monolayer.

To gain insight into the band structure of the γ-B_{28} monolayer, first-principles calculations within the HSE06 hybrid functional were performed on the electronic band structure to determine the exchange-correlation potential. It was found that monolayer γ-B_{28} is a promising direct band gap semiconductor with a band gap of 2.07 eV at the Γ point between the valence band maximum and the conduction band minimum (Figure 4 c). As usual, the first-principles calculations underestimated the band gap, so the theoretical value is in reasonable agreement with the measured optical band gap of 2.25 eV. The projected density of states (PDOS) of the monolayer is shown in Figure 4 d. Strong hybridization between the s and p orbitals of the boron atoms is observed, especially in the valence bands, but the p orbital dominantly contributes to the total DOS. The monolayer exhibits a direct band gap semiconductor character, predominantly owing to the out-of-plane states (p orbitals) of the unsaturated B_p atoms, which are located at the bottom of the conduction band. Compared with the indirect band gap (1.7 eV) of bulk γ-B_{28} calculated by first-principles calculations, such a direct band gap transition gives rise to a large light absorption coefficient.

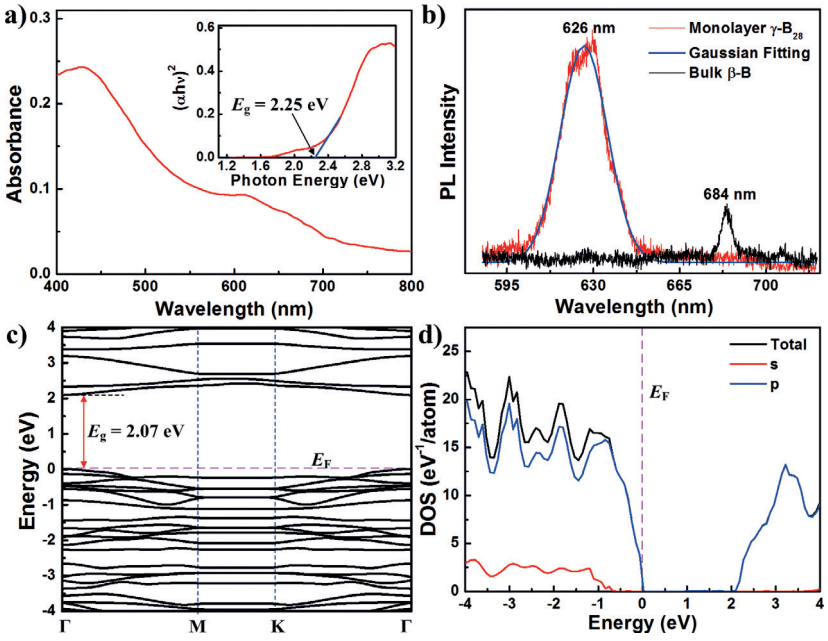

Figure 4. a) UV/Vis absorption spectrum of a monolayer γ-B_{28} film. Inset: $(\alpha h\nu)^2$ as a function of $h\nu$ for band gap determination. b) Photoluminescence spectra of a monolayer γ-B_{28} film and bulk β-rhombohedral boron. The blue line is the corresponding Gaussian fit. c) The electronic band structure of monolayer γ-B_{28}. The Fermi level is indicated by the pink dashed line. d) Calculated total density of states (black line) as well as the local density of states for the s (red line) and p (blue line) orbitals. The energies are given with respect to the valence band maximum (VBM).

In summary, we have reported the synthesis of atomically thin two-dimensional γ-orthorhombic boron films on copper foils by chemical vapor deposition at low pressures. An optical band gap of around 2.25 eV was measured, which is close to the value (2.07 eV) determined by first-principles calculations. Strong photoluminescence is also observed, which suggests that the monolayer is a fascinating direct band gap semiconductor. Our work could pave the way for a variety of explorations towards the application of such boron films in nanoelectronic and nanophotonic devices.

Acknowledgements

This work was supported by the NSF (61474063 and 11302100), Jiangsu NSF (SBK2015022205), the Innovation Fund of

NUAA (NS2013095, NE2015102, NJ20140002, and NZ2015101), the SKL Funding of NUAA (0413Y02 and 0415G02), and the Priority Academic Program Development of Jiangsu Higher Education Institutions. We thank Y. Xiao and Y. W. Ma for valuable discussions.

Keywords: boron · chemical vapor deposition · direct band gaps · monolayers · thin films

How to cite: *Angew. Chem. Int. Ed.* **2015**, *54*, 15473 – 15477
Angew. Chem. **2015**, *127*, 15693 – 15697

[1] G. Fiori, F. Bonaccorso, G. Iannaccone, T. Palacios, D. Neumaier, A. Seabaugh, S. K. Banerjee, L. Colombo, *Nat. Nanotechnol.* **2014**, *9*, 768 – 779.
[2] a) D. C. Elias, R. R. Nair, T. M. G. Mohiuddin, S. V. Morozov, P. Blake, M. P. Halsall, A. C. Ferrari, D. W. Boukhvalov, M. I. Katsnelson, A. K. Geim, K. S. Novoselov, *Science* **2009**, *323*, 610 – 613; b) R. Balog, B. Jorgensen, L. Nilsson, M. Andersen, E. Rienks, M. Bianchi, M. Fanetti, E. Laegsgaard, A. Baraldi, S. Lizzit, Z. Sljivancanin, F. Besenbacher, B. Hammer, T. G. Pedersen, P. Hofmann, L. Hornekaer, *Nat. Mater.* **2010**, *9*, 315 – 319.
[3] R. Lv, J. A. Robinson, R. E. Schaak, D. Sun, Y. F. Sun, T. E. Mallouk, M. Terrones, *Acc. Chem. Res.* **2015**, *48*, 56 – 64.
[4] S. Das, J. A. Robinson, M. Dubey, H. Terrones, M. Terrones, *Annu. Rev. Mater. Res.* **2015**, *45*, 1 – 27.
[5] C. N. R. Rao, H. S. S. R. Matte, U. Maitra, *Angew. Chem. Int. Ed.* **2013**, *52*, 13162 – 13185; *Angew. Chem.* **2013**, *125*, 13400 – 13424.
[6] B. Radisavljevic, A. Radenovic, J. Brivio, V. Giacometti, A. Kis, *Nat. Nanotechnol.* **2011**, *6*, 147 – 150.
[7] a) S. L. Zhang, Z. Yan, Y. F. Li, Z. F. Chen, H. B. Zeng, *Angew. Chem. Int. Ed.* **2015**, *54*, 3112 – 3115; *Angew. Chem.* **2015**, *127*, 3155 – 3158; b) S. Cahangirov, M. Topsakal, E. Akturk, H. Sahin, S. Ciraci, *Phys. Rev. Lett.* **2009**, *102*, 236804; c) L. K. Li, Y. J. Yu, G. J. Ye, Q. Q. Ge, X. D. Ou, H. Wu, D. L. Feng, X. H. Chen, Y. B. Zhang, *Nat. Nanotechnol.* **2014**, *9*, 372 – 377; d) Y. Xu, B. H. Yan, H. J. Zhang, J. Wang, G. Xu, P. Z. Tang, W. H. Duan, S. C. Zhang, *Phys. Rev. Lett.* **2013**, *111*, 136804; e) L. Z. Kou, Y. D. Ma, X. Tan, T. Frauenheim, A. J. Du, S. Smith, *J. Phys. Chem. C* **2015**, *119*, 6918 – 6922; f) L. Tao, E. Cinquanta, D. Chiappe, C. Grazianetti, M. Fanciulli, M. Dubey, A. Molle, D. Akinwande, *Nat. Nanotechnol.* **2015**, *10*, 227 – 231.
[8] a) Y. M. Shi, H. N. Li, L. J. Li, *Chem. Soc. Rev.* **2015**, *44*, 2744 – 2756; b) Q. Q. Ji, Y. Zhang, Y. F. Zhang, Z. F. Liu, *Chem. Soc. Rev.* **2015**, *44*, 2587 – 2602.
[9] M. C. Hersam, *ACS Nano* **2015**, *9*, 4661 – 4663.
[10] E. Gibney, *Nature* **2015**, *522*, 274 – 276.
[11] a) B. Albert, H. Hillebrecht, *Angew. Chem. Int. Ed.* **2009**, *48*, 8640 – 8668; *Angew. Chem.* **2009**, *121*, 8794 – 8824; b) J. F. Tian, Z. C. Xu, C. M. Shen, F. Liu, N. S. Xu, H. J. Gao, *Nanoscale* **2010**, *2*, 1375 – 1389; c) A. P. Sergeeva, I. A. Popov, Z. A. Piazza, W. L. Li, C. Romanescu, L. S. Wang, A. I. Boldyrev, *Acc. Chem. Res.* **2014**, *47*, 1349 – 1358; d) M. I. Eremets, V. W. Struzhkin, H. K. Mao, R. J. Hemley, *Science* **2001**, *293*, 272 – 274.
[12] A. R. Oganov, J. H. Chen, C. Gatti, Y. Z. Ma, Y. M. Ma, C. W. Glass, Z. X. Liu, T. Yu, O. O. Kurakevych, V. L. Solozhenko, *Nature* **2009**, *457*, 863 – 867.
[13] a) M. H. Evans, J. D. Joannopoulos, S. T. Pantelides, *Phys. Rev. B* **2005**, *72*, 045434; b) J. Kunstmann, A. Quandt, *Phys. Rev. B* **2006**, *74*, 035413; c) I. Boustani, *Surf. Sci.* **1997**, *370*, 355 – 363.
[14] X. J. Wu, J. Dai, Y. Zhao, Z. W. Zhuo, J. L. Yang, X. C. Zeng, *ACS Nano* **2012**, *6*, 7443 – 7453.
[15] a) Z. A. Piazza, H. S. Hu, W. L. Li, Y. F. Zhao, J. Li, L. S. Wang, *Nat. Commun.* **2014**, *5*, 3113; b) E. S. Penev, S. Bhowmick, A. Sadrzadeh, B. I. Yakobson, *Nano Lett.* **2012**, *12*, 2441 – 2445; c) W. L. Li, Q. Chen, W. J. Tian, H. Bai, Y. F. Zhao, H. S. Hu, J. Li, H. J. Zhai, S. D. Li, L. S. Wang, *J. Am. Chem. Soc.* **2014**, *136*, 12257 – 12260; d) X. F. Zhou, A. R. Oganov, X. Shao, Q. Zhu, H. T. Wang, *Phys. Rev. Lett.* **2014**, *112*, 085502.
[16] a) Y. Y. Liu, E. S. Penev, B. I. Yakobson, *Angew. Chem. Int. Ed.* **2013**, *52*, 3156 – 3159; *Angew. Chem.* **2013**, *125*, 3238 – 3241; b) Z. H. Zhang, Y. Yang, G. Y. Gao, B. I. Yakobson, *Angew. Chem. Int. Ed.* **2015**, *54*, 13022 – 13026; *Angew. Chem.* **2015**, *127*, 13214 – 13218; c) H. S. Liu, J. F. Gao, J. J. Zhao, *Sci. Rep.* **2013**, *3*, 3238.
[17] E. Y. Zarechnaya, L. Dubrovinsky, N. Dubrovinskaia, N. Miyajima, Y. Filinchuk, D. Chernyshov, V. Dmitriev, *Sci. Technol. Adv. Mater.* **2008**, *9*, 044209.
[18] E. Y. Zarechnaya, L. Dubrovinsky, N. Dubrovinskaia, Y. Filinchuk, D. Chernyshov, V. Dmitriev, N. Miyajima, A. El Goresy, H. F. Braun, S. Van Smaalen, I. Kantor, A. Kantor, V. Prakapenka, M. Hanfland, A. S. Mikhaylushkin, I. A. Abrikosov, S. I. Simak, *Phys. Rev. Lett.* **2009**, *102*, 185501.
[19] L. F. Wang, B. Wu, J. S. Chen, H. T. Liu, P. A. Hu, Y. Q. Liu, *Adv. Mater.* **2014**, *26*, 1559 – 1564.
[20] J. Kotakoski, C. H. Jin, O. Lehtinen, K. Suenaga, A. V. Krasheninnikov, *Phys. Rev. B* **2010**, *82*, 113404.
[21] a) E. Zarechnaya, N. Dubrovinskaia, R. Caracas, M. Merlini, M. Hanfland, Y. Filinchuk, D. Chernyshov, V. Dmitriev, L. Dubrovinsky, *Phys. Rev. B* **2010**, *82*, 184111; b) E. Y. Zarechnaya, N. Dubrovinskaia, L. Dubrovinsky, *High Pressure Res.* **2009**, *29*, 530 – 535.
[22] H. Werheit, V. Filipov, U. Kuhlmann, U. Schwarz, M. Armbruster, A. Leithe-Jasper, T. Tanaka, I. Higashi, T. Lundstrom, V. N. Gurin, M. M. Korsukova, *Sci. Technol. Adv. Mater.* **2010**, *11*, 023001.
[23] H. Z. Zhuang, X. W. Zou, Z. Z. Jin, D. C. Tian, *Phys. Rev. B* **1997**, *55*, R6105.
[24] W. C. Foo, J. S. Ozcomert, M. Trenary, *Surf. Sci.* **1991**, *255*, 245 – 258.
[25] T. T. Xu, J. G. Zheng, N. Q. Wu, A. W. Nicholls, J. R. Roth, D. A. Dikin, R. S. Ruoff, *Nano Lett.* **2004**, *4*, 963 – 968.
[26] T. R. Burkholder, L. Andrews, *J. Chem. Phys.* **1991**, *95*, 8697 – 8709.
[27] A. Y. Lozovoi, A. T. Paxton, *Phys. Rev. B* **2008**, *77*, 165413.
[28] J. S. Gillespie, *J. Am. Chem. Soc.* **1966**, *88*, 2423 – 2425.

Received: October 5, 2015
Published online: October 28, 2015

